P 154

Joint inversion of 3D seismic and Towed Streamer EM facilitating estimates of total hydrocarbon volume in place

Folke Engelmark and Johan Mattsson*

Summary

In October 2012 a medium sized oil & gas field in the Norwegian sector of the North Sea was successfully detected using Towed Streamer EM. It is a challenging target for EM methods, since it is located 2,100 m below mudline, and approximately half of the recoverable oil has been produced with the gas-cap still intact. The hydrocarbon column is approximately 53 m thick with a 25 m gas column over 28 m of oil.

The 800 m long bipole source was towed at a depth of 10 m with a signal strength of 1.2 MAm. The EM streamer was 8,700 m long and towed at a depth of 50 m. The resulting electric field was measured at 23 offsets ranging from 500 to 7,700 m. The towing speed was 4 knots, and the water depth was 110 – 125 m. Following processing the maximum anomaly was found to be 8 % above background with an estimated uncertainty of +/- 3 %.

Using 3D seismic to build a sparse structural layer-model to constrain the inversion allows us to estimate the vertical and horizontal resistivity directly from the data for all the rock volumes from sea-level down to below the reservoir. In addition, the inversion provides an estimate of the anisotropy of the charged reservoir interval facilitating an estimate of net-to-gross as well as resistivity of the charged reservoir sands. The final result is an improved quantitative estimate of the total hydrocarbon volumes in place.

Keywords: *CSEM, marine EM, acquisition, inversion, towed EM*

Introduction

Controlled source electro-magnetic (CSEM) marine methods have traditionally been node-based systems, where the receivers are placed as autonomous recording stations on the seafloor in a very sparse line or areal pattern. The source is then towed close to the seafloor emitting a constant source signal, which is typically a monochromatic square-wave.

The first available towed streamer EM system was tested in its final form in October 2012. The similarities to marine seismic acquisition are obvious, and the advantages are many including acquisition speed at 4-5 knots, fixed source - receiver geometry, dense common mid-point (cmp) sampling, real-time quality control and on-board processing facilitating a quick-look at the transverse resistance of the reservoir.

The Alvheim – Boa reservoir, known as the Heimdal sandstone, is a challenging target due to average areal extent and a depth of burial at 2,100 m below mudline. The reservoir is a submarine fan. They are notoriously difficult to evaluate, even in wireline log data, and often show a rather low net-to-gross (N/G). A weak but consistent anomaly is seen in the towed streamer EM data next to the depocenter, and most significant is that a series of 1D cmp inversions along the survey lines requires a strong anisotropy to be assigned to the reservoir, in order for the inversion to converge properly. The anisotropy is not necessarily intrinsic to any lithology but arises mainly as an effective anisotropy from the architecture of submarine fan reservoirs, where the highly resistive hydrocarbon-charged sands are inter-bedded with low resistivity shales. With the estimated vertical and horizontal resistivities within the reservoir, together with an estimate of the shale resistivity, the resistivity of the sands can be

Petroleum Geo-Services, 111 Somerset Road #15-05/06, Singapore 238164,
folke.engelmark@pgs.com

estimated together with an estimate of the net-to-gross (N/G).

The towed streamer EM acquisition system

The layout of the acquisition system when configured for simultaneous EM and 2D seismic acquisition is shown in Figure 1 below.

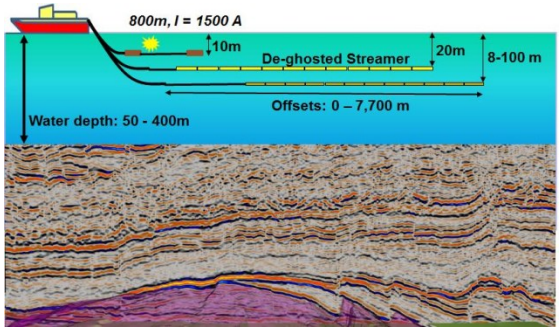

Figure 1: The layout of the acquisition system configured for simultaneous acquisition of EM and 2D seismic. The 800 m long bi-pole is towed at 10 m emitting a 1,500 A source signal. The EM streamer has 23 offsets from 0 – 7,700 m and it is towed at a nominal depth of 100 m. The de-ghosted seismic streamer is towed at 20 m and the towing speed is 4 – 5 knots.

The bi-pole source is 800 m long and towed at a depth of 10 m. The source runs at 1,500 A, and the source signal is user selectable. Our current favorite is the so-called Optimized Repeated Sequence (ORS). It can be viewed as a square-wave with twice the density of the discrete harmonics seen in a monochromatic square-wave. The signal sequence is 120 s long with the source active the first 100 s followed by 20 s of no signal that is used for background noise estimation and noise reduction processing. The maximum nominal water depth is 400 m. Larger water depths are acceptable provided the reservoir is large, has a high transverse resistance, or is shallow below mudline.

A number of different noise reduction methods have been implemented as described by Mattsson et al (2012). Stochastic noise is attenuated in two different ways. First the dense sampling both within the streamer and along the survey lines facilitates noise reduction by stacking that improves S/N by a factor $N^{1/2}$, where N is the number of stacked signals. The second method is known as the low rank approximation based on singular value decomposition. It takes advantage of the fact that the signal only occupies discrete frequencies, whereas the stochastic noise is spread throughout the spectrum. By identifying the discrete signal frequencies, all noise between these frequencies can be removed.

Estimating the uncertainty in the frequency response data as a function of signal frequency and offset is an important aspect of the processing and analysis of the acquired data. The signal needs to exceed the noise level to be recognized as signal with confidence. Noise, or uncertainty, originates in the measurement system, navigation and the electric field noise in the measurement. The total uncertainty in the frequency response data was calculated as seen in Figure 2 (amplitude) and Figure 3 (phase) below for data acquired at the Alvheim Boa field (described below) in the North Sea. The maximum relative amplitude uncertainty is seen to be below 5% for the amplitude and below 3% for the phase.

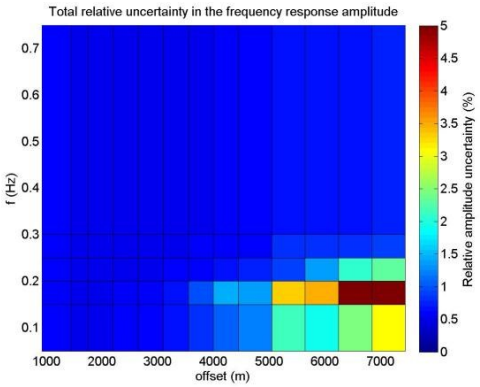

Figure 2. The total relative uncertainty in the frequency response amplitude.

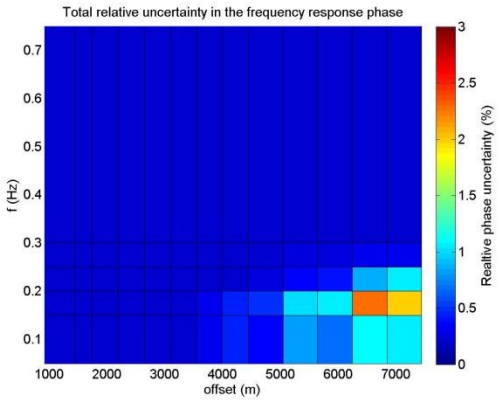

Figure 3. The total relative uncertainty in the frequency response phase.

The dominant part of the uncertainty is coming from the electric field noise for the low frequencies and long offsets. The sum of measurement and navigation uncertainties is below 1% and influences the total uncertainty only where it is very low, i. e., in the higher frequencies and shorter offsets.

The Alvheim-Boa towed streamer EM data acquisition

The Alvheim-Boa reservoir was deposited as a submarine fan, and it is located at 2,100 m below mudline in 110 – 125 m water depth. The two sub-parallel survey lines strike in the NNE direction over the Boa reservoir as seen in Figure 4.

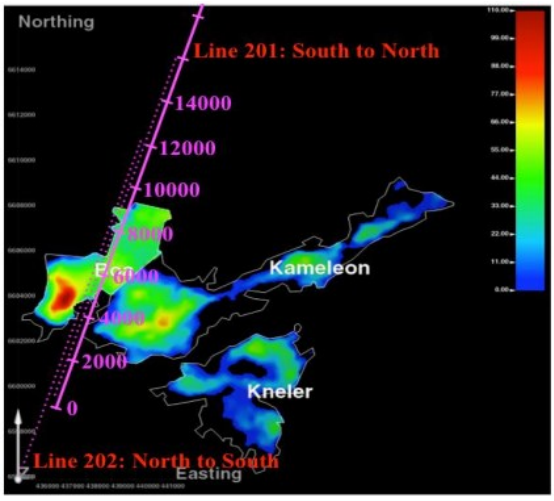

Figure 4: The Alvheim – Boa oil and gas field. The two survey lines are shown as magenta dotted lines. The Boa depocenter mapped from seismic is seen as the red anomaly immediately to the left of the lines. The color scale shows the reservoir thickness in meters. The solid magenta line is a reference line labeled in meters common to both lines.

The location of the lines is suboptimal due to permit constraints and existing infrastructure in the area, but they are traversing close to the Boa depocenter as mapped from the seismic data and seen in warm colors to the left of the survey lines shown as magenta dotted lines. Immediately to the right of the survey lines is a reference line showing the common distance for both lines from an arbitrary point outside the reservoir. The direction of sailing is also shown as south to north for Line 201 and north to south for Line 202.

It is valuable to be able to estimate the resistivity profile of the overburden as a calibration for the inversion of the EM data. In a clastic environment where the overburden consists of inter-bedded sands and shales, the shales tend to dominate the sequence. Hence, if we can estimate the expected shale resistivity trend as a function of seismic velocities, an upper bound in the resistivity trend can be established for the overburden. If pre-stack inverted data is available, the overburden can be subdivided into sands and shales, and separate transforms from velocity to resistivity can be developed for both lithologies. The relationship between velocity and resistivity for sands is well understood but not for shales. Figure 5 shows the deep induction log (red) from well 24/6-1 in the field located close to 8,500 m common line location.

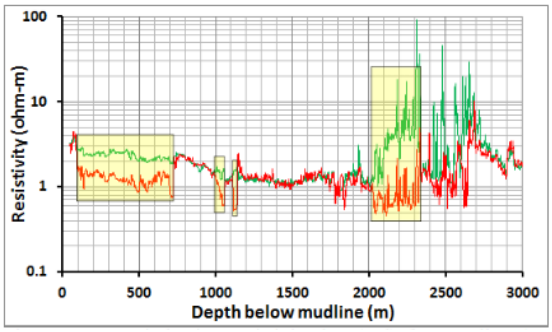

Figure 5: Deep induction resistivity log (red) from well 24/6-1 penetrating the Boa reservoir (2,020 – 2,330 m below mudline) outside the hydrocarbon charged volume. The green curve is a shale-resistivity model based on logged velocity. Highlighted in yellow are the Utsira sand (shallow) and the Heimdal reservoir (deep) where the shale model deviates from the logged data as expected.

The reservoir is not hydrocarbon charged in this location. The green curve is a velocity to shale-resistivity transform based on the sonic log as described in Engelmark (2010). The yellow highlights mark the Utsira sand (100 – 710 m) and the Heimdal sand, which is the Alvheim – Boa reservoir (2040 – 2320 m). The shale model deviates from the logged resistivity in the sands as expected. The deep induction log shown here measures the horizontal resistivity. Modern tri-axial tools that simultaneously measure vertical and horizontal resistivity have been introduced, but are still rarely used.

Inverting to resistivity

The vertical and horizontal resistivities below mud-line were estimated by means of 1D multi-trace anisotropic inversions for each cmp along the survey lines. The 1D inversions were then concatenated to show the resistivity as a continuous 2D profile along each line. The inversion is formulated as a minimization problem using a trust-region- reflective algorithm based on the interior-reflective algorithm described by Coleman and Li (1994, 1996). The associated frequency response uncertainties are used in the weights to down-scale the noisy data.

For both survey lines a twelve-layer model was estimated at each cmp. The bathymetry was estimated from echo sounder measurements on board the vessel and the seawater conductivity was included in the inversion. The water depth varies from 110 m in the north of the lines to 125 m in the south area. Interpreted stratigraphic surfaces in the seismic cross sections were used as the only constraints in the inversion of the resistivities below mudline. The Heimdal reservoir itself, also mapped in depth and thickness according to the well log, was then discretized into seven layers each 70 m thick followed by a half-space of under- burden. All subsurface layer thicknesses were kept fixed during the inversions, and it is only the vertical and horizontal resistivities that were inverted for.

Frequency response data at six frequencies between 0.05 and 0.75 Hz and eight offsets ranging 1,700 m to 7,700 m were used for all the inversions. This data set enables sufficient sensitivity for both the vertical and horizontal resistivity from the mud-line down to 2,600 m into the subsurface. The minimum detectable resistivity change in each layer given the corresponding total uncertainty in the data is shown in Figure 6.

It is clearly seen that the selected in-line data has roughly the same sensitivity for both the vertical and horizontal resistivity. The relatively thick overburden layers imply a resolution below 0.1 ohm-m. The smallest possible detectable resistivity change within the thinner layers of the reservoir is about 1 ohm-m, which is sufficient to resolve the resistivity increase in the hydrocarbon filled reservoir layers. Even though shorter offsets were recorded, they were neglected in the data going into the inversion. The reason is that a more finely resolved subsurface depth model is necessary to capture the variations that are relevant to these short offsets. However, to roughly estimate the overburden and characterize the deeper anomalous region in detail, the offsets from 1,700 – 7,700 m are sufficient.

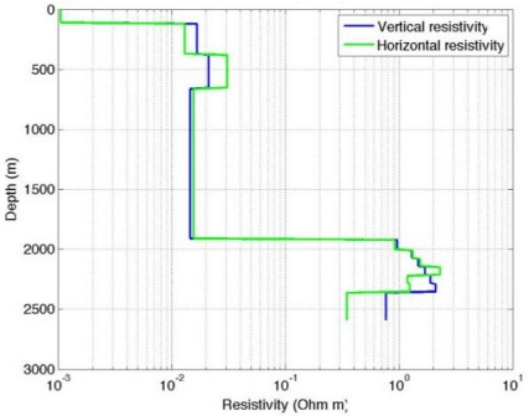

Figure 6. The resulting sensitivity with respect to vertical (blue) and horizontal (green) resistivity expressed as minimum detectable change in resistivity for each layer.

The relative difference, or misfit, between the measured and the modeled frequency responses after inversion were plotted as a function of offset and frequency for both the amplitude and the phase. The results for the relative difference in the amplitude and phase, shown in Figure 7 and Figure 8 respectively, are largely below 4%. These values are at similar levels as the residual noise in the field data after processing, hence providing a natural lower limit in the minimization process of the measured to modeled difference.

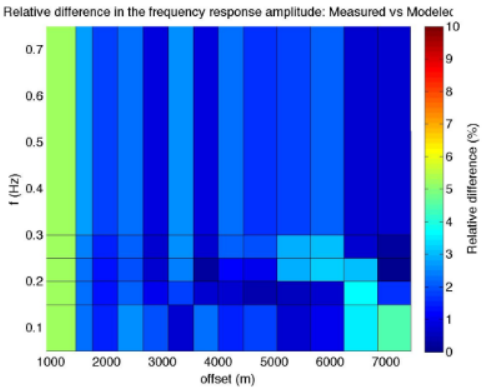

Figure 7. Example of the relative difference between measured and modeled frequency response amplitude.

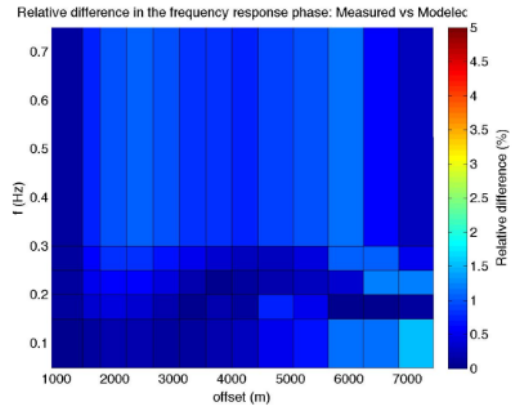

Figure 8. Example of the relative difference between measured and modeled frequency response phase.

Converting resistivity to oil & gas in place

Following the inversion, the resulting vertical and horizontal resistivity cross sections are shown in Figure 9 and Figure 10 respectively for Line 201.

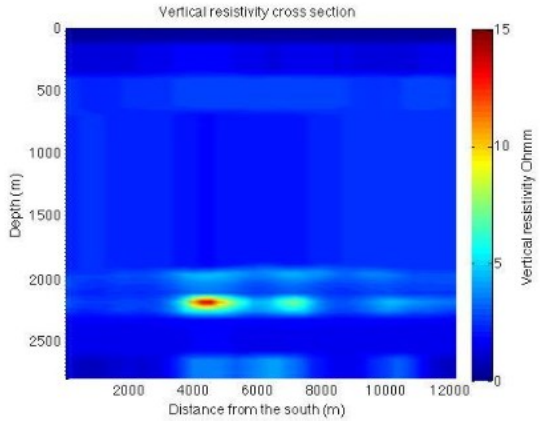

Figure 9. The estimated vertical resistivity for Line 201.

Neither line traverses the depocenter but Line 201 is somewhat closer than Line 202, hence likely to be more representative. The locations of the anomalies coincide well with the maximum seismic amplitude as seen in Figure 3. The vertical resistivity rises to 18 ohm-m within the reservoir and the horizontal resistivity increases to 3 ohm- m at the same depth interval resulting in an anisotropy ratio of 6. Hence, even in a rather thin reservoir layer there is sensitivity to the horizontal component in the inline data. In comparison the vertical and horizontal resistivities in the proximal overburden are estimated to 2.3 and 1.4 ohm-m, respectively, resulting in an anisotropy ratio of 1.6.

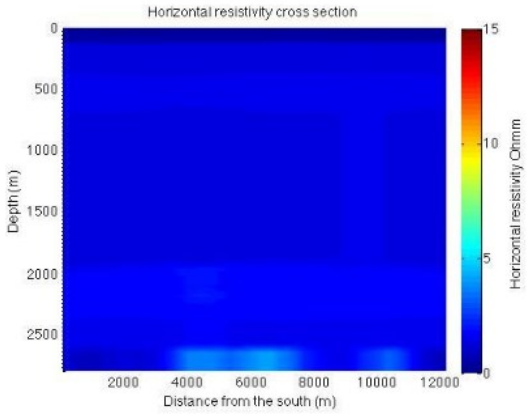

Figure 10. The estimated horizontal resistivity for Line 201.

The vertical resistivity R_v is the volumetrically weighted arithmetic average

$$R_v = V_{sh}R_{sh} + V_{sd}R_{sd}$$

The horizontal resistivity R_h is the volumetrically weighted harmonic average:

$$\frac{1}{R_h} = \frac{V_{sh}}{R_{sh}} + \frac{V_{sd}}{R_{sd}}$$

where V_{sh} = shale volume; R_{sh} = shale resistivity; V_{sd} = sand volume; and R_{sd} = sand resistivity.

The analysis can then be further pursued by using three known reference data points:

1. The resistivity is known for the shales within the reservoir from well logs in the area. The horizontal resistivity averages 1.1 ohm-m and with an average expected shale anisotropy of 2.0, the vertical resistivity of the shales can be expected to be ~2.2 ohm-m.
2. The vertical resistivity for the charged reservoir is estimated at 18 ohm-m.
3. The horizontal resistivity for the charged reservoir is estimated at 3 ohm-m.

This is sufficient information to draw up an analysis such as the one seen in Figure 11, where the straight red line (arithmetic average) represents the vertical resistivity as a function of N/G, and the blue line (harmonic average) at the bottom with the dramatic rise to the right represents the horizontal resistivity as a function of N/G.

The sand is assumed to be isotropic, whereas the shale is represented as anisotropic (2.2 & 1.1 ohm-m). Based on the shale resistivity and the inverted vertical and horizontal resistivities within the reservoir, there is a unique solution for sand resistivity of 26.2 ohm-m and a N/G of 0.66.

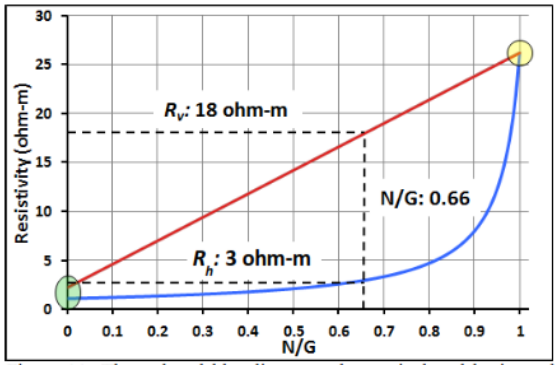

Figure 11: The red and blue lines are the vertical and horizontal resistivity, respectively, as a function of N/G. Four points are known: the anisotropic shale resistivities (2.2 & 1.1 ohm-m) to the lower left circled in green, and the vertical and horizontal resistivities for the reservoir at 18 and 3 ohm-m respectively. This allows us to uniquely estimate N/G at 0.66 and the resistivity of the sands at 26.2 ohm-m.

All the information is now available to estimate the total hydrocarbon volume in place:

1. Sand resistivity and N/G from the analysis shown in Figure 11.
2. Sand porosity and brine resistivity (R_w) from well logs. If there are no wells in the area, the porosity can be estimated from inverted seismic data. R_w can then be estimated based on an assumed salinity of seawater and an estimated temperature gradient.
3. Total charged reservoir volume from depth converted seismic data. With the hydrocarbon-charged sand resistivity R_t, the sand porosity ϕ and R_w from the well logs, it is now possible to estimate the water saturation S_w, and hence also the hydrocarbon saturation S_{hc} in the sands based on the Archie equation:

$$S_{hc} = 1 - S_w = 1 - \left(\frac{a \cdot R_w}{\phi^m \cdot R_t} \right)^{1/n}$$; where a: tortuosity (0.81), R_w: pore water resistivity, m: cementation exponent (2.0), and n: the saturation exponent (2.0).

The hydrocarbon pore volume (HPV) is then:

$$HPV = S_{hc} \cdot \phi$$

By incorporating the N/G and the total gross reservoir volume V_{res} from the depth converted seismic, the total hydrocarbon volume in place HCV_{tot} is then:

$$HCV_{tot} = HPV \cdot N/G \cdot V_{res}$$

The ability to evaluate both vertical and horizontal resistivity is also very important when evaluating a reservoir in the vicinity of, or directly on top of, a high resistivity basement or other resistive body. This has traditionally been considered a difficult problem to resolve. However, the basement is assumed to be either isotropic, or display inverse anisotropy where the horizontal resistivity is larger than the vertical, as would be the case if the basement is fractured. Vertical fractures are expected to be more frequent and with a wider aperture facilitating better conductivity than the horizontal fractures. Hence, if the charged reservoir shows strong anisotropy, it can be uniquely identified and outlined based on the anisotropy alone.

Conclusions

The Alvheim – Boa reservoir is a challenging target due to the combination of depth below mudline (2,100 m), limited lateral extension of the depocenter (2,000 m) and a low to average transverse resistance of the charged reservoir. An additional weakness is the suboptimal positioning of the survey lines that traverse off the side of the depocenter further reducing the signal and adding uncertainty. Due to the lack of data from the central part of the charged reservoir, it was decided not to perform 2 ½ D inversion. Instead, as a proof of concept, a series of fast 1D inversions were concatenated to form continuous 2D lines, facilitating an estimate of maximum vertical and horizontal resistivity in the reservoir. The vertical and horizontal resistivity together with an estimated shale resistivity facilitates an extraction of charged sand resistivity and N/G. With porosity and brine resistivity estimated in the wells, the hydrocarbon saturation can be estimated based on Archie's equation. This together with the porosity, N/G and total charged reservoir volume mapped from depth-converted seismic yields an estimate of the total hydrocarbon volumes in place.

In addition, the fact that vertical and horizontal resistivity can be estimated from the towed streamer EM data facilitates detection of a strongly anisotropic reservoir even when it is located immediately on top of basement. The basement is expected be isotropic, or possibly show reversed anisotropy based on the more frequent vertical fractures that are also likely to be more open, hence also more conductive. In such a situation, the reservoir can be confidently detected and outlined based on anisotropy alone.

Acknowledgements

We thank Petroleum Geo-Services for the permission to present this work.

References

Archie, G. E., 1942, The electrical resistivity log as an aid in determining some reservoir characteristics: Journal of Petroleum Technology, v. 5, p. 54-62.

T F Coleman and Li Y, An Interior, Trust Region Approach for Nonlinear Minimization Subject to Bounds, SIAM Journal on Optimization, Vol. 6, pp. 418–445, 1996.

T F Coleman and Li Y, On the Convergence of Reflective Newton Methods for Large-Scale Nonlinear Minimization Subject to Bounds, Mathematical Programming, Vol. 67, Number 2, pp. 189–224, 1994.

Engelmark, F., 2010, Velocity to resistivity transform via porosity: 80th SEG Conference & Exhibition, Extended Abstracts 2010.

Mattsson, J., Lindqvist, P., Juhasz, R., Björnemo, E., 2012, Noise reduction and error analysis for a towed EM system: 82nd SEG Conference & Exhibition, Extended Abstract.